Journal of Applied Physics

Hydrogen-related defects measured by infrared spectroscopy in multicrystalline silicon wafers throughout an illuminated annealing process

Cite as: J. Appl. Phys. **127**, 065703 (2020); https://doi.org/10.1063/1.5142476
Submitted: 17 December 2019 . Accepted: 26 January 2020 . Published Online: 10 February 2020

Philip M. Weiser, Eduard Monakhov, Halvard Haug, Marie Syre Wiig, and Rune Søndenå

Journal of Applied Physics ARTICLE scitation.org/journal/jap

Hydrogen-related defects measured by infrared spectroscopy in multicrystalline silicon wafers throughout an illuminated annealing process

Cite as: J. Appl. Phys. **127**, 065703 (2020); doi: 10.1063/1.5142476
Submitted: 17 December 2019 · Accepted: 26 January 2020 ·
Published Online: 10 February 2020

Philip M. Weiser,[1] Eduard Monakhov,[1] Halvard Haug,[1,2] Marie Syre Wiig,[2] and Rune Søndenå[2,a)]

AFFILIATIONS

[1]Centre for Materials Science and Nanotechnology, Department of Physics, University of Oslo, P.O. Box 1048, Blindern, 0316 Oslo, Norway
[2]Institute for Energy Technology, Instituttveien 18, 2007 Kjeller, Norway

[a)]**Author to whom correspondence should be addressed:** Rune.Sondena@ife.no

ABSTRACT

Hydrogen (H) is thought to be strongly involved in the light and elevated temperature-induced degradation observed predominantly in p-type silicon wafers, but the nature of the defect or defects involved in this process is currently unknown. We have used infrared (IR) spectroscopy to detect the vibrational signatures due to the H–B, H–Ga, and H_2*(C) defects in thin, hydrogenated, p-type multicrystalline silicon wafers after increasing the optical path length by preparation and polishing the edges of a stack of wafers. The concentrations of the H–B and H–Ga acceptor complexes are reduced to 80% of their starting values after low intensity (5 mW/cm^2) illumination at room temperature for 96 h. Subsequent high intensity illumination (70 mW/cm^2) at 150 °C for 7–8 h further decreases the concentrations of these defects; to ∼40% (H–B) and ∼50% (H–Ga) of their starting values. Our results show that, with careful sample preparation, IR spectroscopy can be used in conjunction with other techniques, e.g., quasisteady-state photoconductance, to investigate the involvement of different H-related point defects on degradation in solar-grade silicon wafers.

I. INTRODUCTION

Hydrogen (H) can passivate and neutralize a wide range of defects and impurities in crystalline silicon, such as metallic impurities, grain boundaries, and dislocations.[1–7] Thus, hydrogen introduction, also called hydrogenation, and the corresponding beneficial effects on the minority carrier lifetimes in silicon wafers is important for the performance of crystalline silicon solar cells. Hydrogen can be introduced into the bulk silicon in several ways; high temperature processing in a hydrogen atmosphere,[8] ion implantation,[9] plasma treatment,[10] and release of hydrogen from a dielectric layer.[11,12] This last method is the most common method in solar cell production, achieved when the metallic contacts are fired through a hydrogen-rich dielectric film, e.g., SiN_X:H, which serves both as a surface passivation layer and an antireflection coating (ARC).[13] In addition to passivating grain boundaries and metallic impurities, H has also been connected to the formation and deactivation of boron–oxygen related defects causing light induced degradation (BO-LID), with a demonstrated effect on the reaction rates.[14,15] Unfortunately, there are also negative effects associated with hydrogenation. Recombination due to hydrogen defects by their own has recently been proposed.[16] The detrimental light and elevated temperature-induced (LeTID) defect, first reported by Ramspeck *et al.*,[17] is also closely related to hydrogen. Hydrogenation, either by plasma injection or by contact firing with a hydrogen-rich dielectric layer present, is required to activate the LeTID defect.[10,18,19] The H content in the ARC as well as the profile and peak temperature of the firing process affects the extent of the LeTID.[20,21] Although the root-cause of LeTID is still unknown, the involvement of hydrogen, either by itself or in a defect complex, is strongly suspected.[10,16,22–24] A defect model including H–B states has recently been proposed to explain the LeTID.[25] In addition, some metallic impurities remain as potential candidates.[22,24,26]

Despite many states and potential effects of hydrogen in the bulk silicon, it is notoriously difficult to observe directly. The concentrations in the bulk are often too low to be detected, e.g., using

secondary ion mass spectrometry (SIMS) even when hydrogen is substituted with deuterium (D) for increased sensitivity.[27] Diatomic forms of hydrogen, which are often electrically and optically inactive, are energetically preferable compared to monatomic forms.[28–32] Thus, only a fraction of hydrogen in silicon is represented by the monatomic hydrogen. Interstitial monatomic hydrogen in silicon can exist in three charge states: positive (H^+), neutral (H^0), and negative (H^-). In the p-type silicon, the H^+ state is predominant,[16,33] which allows it to passivate the electrical activity of, e.g., B- and Ga-acceptors. The issue is complicated even further by the fact that both the thermal history, e.g., quenching, as well as charge injection at elevated temperatures may affect the charge state of hydrogen in silicon.[34,35]

Infrared (IR) absorption spectroscopy is a powerful technique for studying H-related defects in the bulk silicon via their localized vibrational modes (LVMs).[36,37] The LVMs of hydrogen complexes, e.g., with intrinsic defects,[38] transition metals,[39] acceptors,[40] donors,[41,42] as well as other impurities such as carbon,[43,44] have been extensively investigated and are well-documented. In solar cells, the bulk H content has previously been estimated using Fourier Transform-IR (FT-IR) measurements via the reduction of hydrogen in the ARC after firing[18] or indirectly by its effect on the resistivity.[45] The first approach monitored changes in the IR absorption features due to Si–N, Si–H, and N–H before and after the firing process. In the second approach, the changes in the resistivity were assumed to arise from the conversion of *hidden* hydrogen, i.e., hydrogen in dimeric states that give weak or no IR absorbance, into monatomic H^+ which could then neutralize B dopants.[8,34,45] One requires typically high concentrations of light-element impurities, e.g., $10^{18}\,cm^{-3}$ in a 1-μm thick layer or $10^{14}\,cm^{-3}$ in a 1 cm thick layer, in a bulk sample and measurements at cryogenic temperatures to detect their LVMs.[37] For silicon, it is also important to have surfaces polished to optical quality to reduce light scattering. This is a challenge for modern solar cell materials where the defect concentrations are low, the samples are thin, and normal polishing procedures, e.g., mounting the sample in melted wax, can alter the sample state.

In this work, we show that hydrogen-related defect vibrational signatures can be detected in commercially available multicrystalline silicon wafers using FT-IR spectroscopy at cryogenic temperatures. Measurements are performed in the longitudinal direction of a stack of wafers, thus ensuring detectable absorption, and at the same time, suppressing interference effects due to internal reflections. The evolution of the hydrogen content is evaluated in both a hydrogenated and a nonhydrogenated multicrystalline Si wafer at different stages of a degradation–regeneration cycle. Such an approach gives us insight into the H-related point defects that could be connected to the LeTID process.

II. EXPERIMENTAL DETAILS

The samples investigated in this study were cut from a commercially available p-type high performance multicrystalline (HPMC) Si ingot, with a resistivity of about 1.1 Ω cm. Typical concentrations of interstitial oxygen (O_i) and substitutional carbon (C_S), determined from room temperature IR measurements in comparable ingots, are $\sim 2 \times 10^{17}\,cm^{-3}$ and $\sim 5 \times 10^{17}\,cm^{-3}$, respectively.[46] Thin wafers (thickness ~180 μm) were processed in an HNA solution (hydrofluoric, nitric, and acetic acids) to remove saw damage, followed by a two-sided emitter in-diffusion in a $POCl_3$ tube furnace (ca. 70 Ω/sq). Hydrogenation was achieved by plasma enhanced chemical vapor deposition (PECVD) of a dual side dielectric ARC layer (a hydrogen-rich SiN_X-layer) followed by a simulated contact firing step (T_{peak} of about 725 °C) in a belt furnace. Metallic contacts were not applied. Finally, the ARC and the emitter was etched away, and the wafer repassivated with an amorphous silicon/silicon nitride (a-Si/SiN_x) stack, again deposited by PECVD. The process flow is designed to produce samples for lifetime measurements with a low surface recombination velocity (SRV less than 5 cm/s).[47] A nonhydrogenated reference, where a wafer has been damage etched and surface passivated using the a-Si/SiN_x stack without being exposed to the high temperature processes, i.e., the emitter in-diffusion and the simulated contact firing, has also been evaluated. The a-Si/SiN_x stack passivation is also a hydrogen-rich dielectric, but the temperature is limited to 230 °C for a total of 20 min, which should incorporate considerably less hydrogen into the wafer.

Quasisteady-state photoconductance (QssPC) measurements (Sinton lifetime tester WCT-120TS) were performed at room temperature to extract the carrier lifetimes (at an injection level of about $0.1 \times p_0 \approx 1.5 \times 10^{15}\,cm^{-3}$, where p_0 is the thermal equilibrium concentration of holes) on wafer sections halted at different stages of the degradation–regeneration process (see Fig. 2), i.e., all of the wafers start in the same initial state but have different final states. Band-to-band photoluminescence (PL) images were obtained using a LIS-R1 from BT Imaging.[48]

Recently, Wolny *et al.* presented a method to prepare 180 μm-thick monocrystalline wafers that permits evaluation of the O_i concentration at RT.[49] A wafer is broken at cleavage planes at two opposite, parallel edges, resulting in smooth edges that require no additional polishing. Infrared light is then directed at the smooth cleaved edge of a stack of wafers. Unfortunately, this method is not applicable to multicrystalline wafers due to the lack well-defined cleavage planes. We have overcome this limitation by using mechanical polishing. Following QssPC measurements, each section was cut into $1 \times 1\,cm^2$ squares using a process laser. The individual squares were varnished (GE Varnish 7031, Oxford Instruments) on top of one another to create a stack of samples approximately 7 mm in height. One set of parallel edges of the stack were polished to optical quality using successively finer grades of SiC powder (final polish using 5 μm particle size), resulting in a stack width of ~9850 μm. The stacks were soaked in ethanol to remove the varnish and were subsequently cleaned in an ultrasonic bath using acetone, ethanol, and de-ionized water. This procedure allows sample preparation without heating, i.e., without mounting samples in melted wax at ~100 °C. Therefore, the states of the samples are assumed to be unchanged.

Infrared transmittance spectra were acquired using a Bruker IFS 125HR spectrometer equipped with a globar light source, a KBr beam splitter, and a liquid-nitrogen-cooled InSb detector. We utilized the measurement geometry proposed by Wolny *et al.*, in which unpolarized light was directed at normal incidence (±3°) to the polished edges of a stack of silicon squares (see Fig. 1). The samples were cooled to 5.0 K in He exchange gas in a Janis

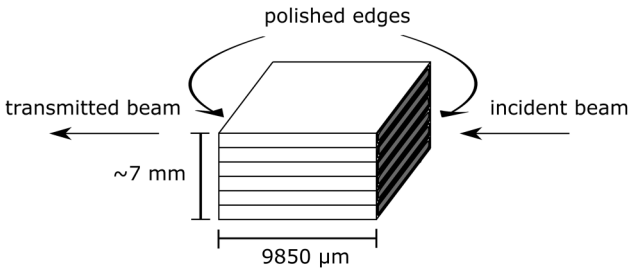

FIG. 1. Schematic view of the sample preparation and the transmittance measurement setup.

PTSHI-950-5 closed cycle, low vibration pulse tube cryostat equipped with ZnSe windows. All measurements were performed with a spectral resolution of 0.5 cm^{-1} and with the empty sample holder serving as the single-channel background spectrum. The transmittance spectra were converted to absorption coefficient spectra by

$$T = \frac{I_{\text{sample}}}{I_{\text{background}}} = \exp(-\alpha d), \tag{1}$$

where T is the transmittance, α is the absorption coefficient of the defect in question, and d is the thickness (or path length) of the sample. The integrated absorption coefficient for each LVM is related to the concentration of the corresponding defect by

$$N_X = \frac{\mu \eta c^2}{\pi q^2} \int \alpha(\bar{\nu}) d\bar{\nu}, \tag{2}$$

where N_X is the concentration of defect X, μ is the reduced mass of the oscillating defect, η is the refractive index, c is the speed of light, q is the effective charge of the oscillator, and $\bar{\nu}$ is the wavenumber.[36] Calibration factors are already available from the literature for the defects identified in these samples and are 3×10^{15} cm^{-1}, 1.76×10^{15} cm^{-1}, and 3.36×10^{17} cm^{-1} for the H–B,[50] H–Ga,[40] and H_2*(C)[43] defects, respectively. An error of about 10% in the absolute defect concentration is expected by neglecting surface reflection effects in Eq. (1).

III. RESULTS AND DISCUSSION

Figure 2 shows the evolution of the QssPC lifetime in a hydrogenated HPMC-Si wafer subjected to a degradation–regeneration process.[19,51] A wafer in the *initial* state has received no additional treatments after the a-Si/SiN_x surface passivation. Illumination at room temperature (RT) under low intensity (5 mW/cm^2) light for 96 h fully activates the BO-LID, and subsequent illumination under a higher intensity (70 mW/cm^2) light at 150 °C for 20 min results in a minimum lifetime, which has been attributed to LeTID.[19,51] These states are referred to as the *BO-degraded* and *LeTID-degraded* states, respectively. Continued illumination under the same conditions (70 mW/cm^2 at 150 °C) for 7–8 h results in a recovery of the lifetime back to its initial value, which is referred to as the

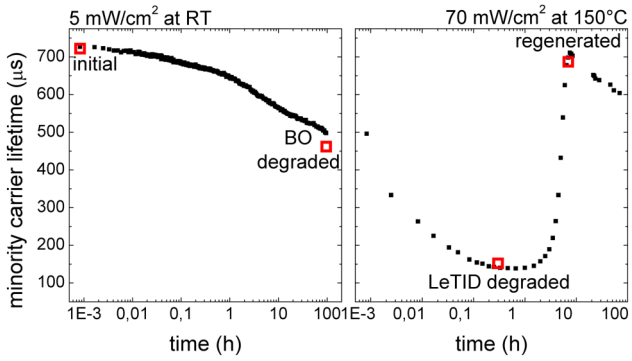

FIG. 2. Time evolution of the minority carrier lifetimes measured with QssPC at a fixed excess carrier density of 1.5×10^{15} cm^{-3} for a hydrogenated HPMC-Si wafer (filled black squares) during the degradation–regeneration process.[19,51] Open red squares represent QssPC measurements on the current wafer subjected to a comparable sequence.

regenerated state. No LeTID degradation was observed in the nonhydrogenated wafer upon the illuminated annealing step.[19] Minority carrier lifetimes measured in sections of a wafer halted at different stages in the degradation–regeneration process, shown as open squares in Fig. 2, correspond well with the continuous lifetime evolution measured on a neighboring wafer. Figure 3 shows room temperature, QssPC-calibrated PL images of hydrogenated wafers at different stages of the degradation–regeneration process. As the 1×1 cm^2 squares used in the stacks are taken from virtually the full area of each of the four wafer sections, we assume that the absorption coefficient spectra and the corresponding defect concentrations

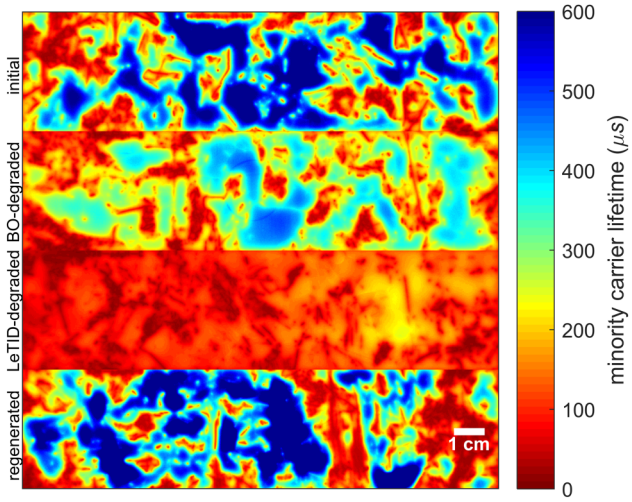

FIG. 3. Carrier lifetime images measured using RT, QssPC-calibrated PL imaging on four sections of the same hydrogenated HPMC-Si wafer at various stages of the degradation- and regeneration processes.

represent an average across the wafer section. Thus, potential spatial differences in bulk hydrogen concentrations due to grain boundaries and dislocation clusters, shown in Fig. 3 as red areas, are neglected in this study.

The IR absorption coefficient spectra for the four different states of the hydrogenated wafer, as well as two states of the nonhydrogenated reference wafer (the *initial* and the *regenerated* state), are shown in Fig. 4. At 5 K, four distinct and previously identified absorption peaks due to Si–H stretch modes are observed, of which two originate from the H–B and H–Ga acceptor complexes[40] at 1904 and 2173 cm^{-1}, respectively, and two from inequivalent configurations of H_2*(C) complexes.[44,52] Absorption peaks at 1922 and 2210 cm^{-1} have been attributed to $CH_{bc}SiH_{ab}$ and $H_{ab}CH_{bc}Si$, where "bc" refers to a bond-centered position and "ab" refers to an antibonding position), respectively. Schematic drawings of the structures can be seen in Ref. 43. Traces of Ga may arise from the use of a small fraction of compensated silicon in the feedstock.[53] The vibrational lines of these defects were not detected in measurements at RT, most likely due to their low concentrations. Furthermore, the H–B and H–Ga vibrational lines are extremely weak in both the *initial* and the *regenerated* states of the nonhydrogenated reference wafers. Thus, a considerably lower hydrogen content in the nonfired wafers is demonstrated. We do not observe any other H-related LVMs, e.g., LVMs associated with the $(CH)_2$ defect,[54] the isolated H_2 molecule,[55–58] the H_2–O_i defect,[59,60] or vacancy–hydrogen complexes,[61–64] in our samples. Khan and co-workers found no link between hydrogen–vacancy complexes and LeTID in a recent study.[65] The absence of hydrogen–vacancy complex LVMs throughout the degradation–regeneration cycle is in agreement with their observations. Current LeTID models consider that the recombination active LeTID defect could also be an isolated metal impurity, in which case the corresponding metal–hydrogen complex would serve as the nonrecombination active precursor defect. Several metal–hydrogen defects have LVMs that fall below the lower range (1850 cm^{-1}) of our InSb detector, as described by Schmidt *et al.*[24] We have made additional measurements (not shown) on our samples using a liquid-nitrogen-cooled MCT detector, which provides a lower spectral limit of 600 cm^{-1}. No metal–hydrogen LVMs were detected in any of the wafer states. Thus, if a metal impurity is responsible for the LeTID, it must be present in the bulk silicon in a low concentration, and its recombination active state must have a corresponding large electron capture cross section in order to explain the detrimental effect on the minority carrier lifetime when fully activated.

Using the vibrational lines shown in the hydrogenated wafer's *initial* state, we calculate concentrations for H–B, H–Ga, and H_2*(C) of $\sim 5 \times 10^{13}$, $\sim 7 \times 10^{13}$, and $\sim 1 \times 10^{15}$ cm^{-3}, respectively. The concentration of B in this wafer was about 1.4×10^{16} cm^{-3} based on the resistivity. Thus, hydrogen passivates approximately 0.5% of the B acceptors. Most of the detected hydrogen, however, is trapped in the form of H_2*(C) defects. Our results are consistent with those of Peng *et al.*,[43] who found that mainly H_2*(C) defects are formed in multicrystalline silicon with $[C_S] \sim 4.9 \times 10^{17}$ cm^{-3}, which is comparable to the expected C_S concentration in our samples. This observation is also consistent with the reported thermal stabilities of H_2*(C), H–B, and H–Ga. Peng *et al.* found that a 30 min anneal at 400 °C removes the vibrational signatures of H_2*(C),[43] whereas the removal of H–B and H–Ga requires considerably lower annealing temperatures, near 300 °C for H–B,[66] and near 200 °C for H–Ga.[67]

Figure 5 shows the evolution of the concentrations of H–B, H–Ga, and H_2*(C) throughout the degradation–regeneration process in two different hydrogenated wafers. The concentrations

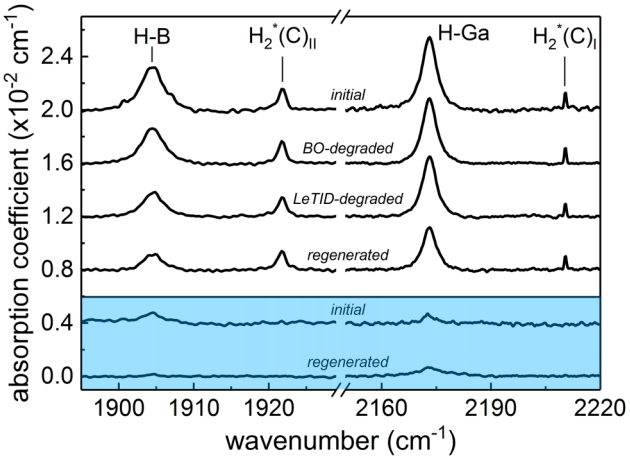

FIG. 4. IR absorption coefficient spectra (5.0 K, res = 0.5 cm^{-1}) of HPMC Si samples (bottom panel = nonhydrogenated, top panel = hydrogenated) in different stages of the degradation–regeneration process. The LVMs of four H-related defects are indicated in the figure. The spectra are vertically offset for clarity and have all been baseline corrected to remove the sloping background.

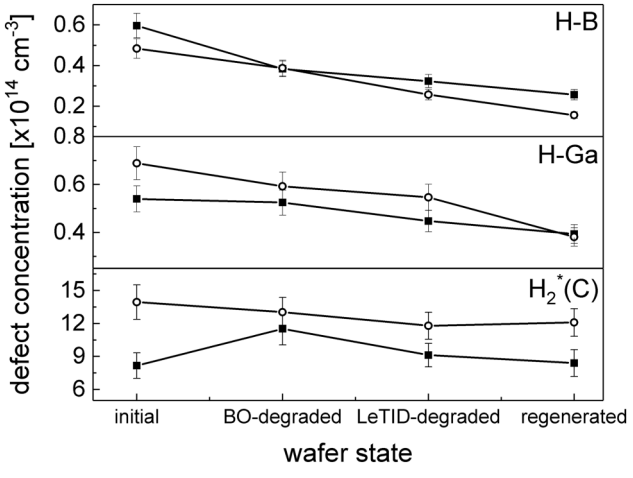

FIG. 5. Concentrations of the H–B, H–Ga, and H_2*(C) defects for different states of the wafers based on the LVMs for two different hydrogenated wafers (the filled squares and open circles represent the two different wafers). The error bars include the 10% uncertainty from neglecting surface reflection effects and the uncertainty in the fits to the integrated absorption coefficients of the vibrational lines. Note that the x axis does not represent a linear time line.

of H–B and H–Ga decrease throughout both illumination processes and reach ~40% and ~50% of their initial values in the regenerated state, respectively. H–Ga bonds seem more stable than H–B bonds, based on the evolution during illumination and annealing. The degradation–regeneration processes affect mainly the H–B and H–Ga defects; the H_2*(C) defects appear to be quite stable against illumination during annealing at both RT and 150 °C. However, as the concentration of H_2*(C) is considerably larger than that of H–B and H–Ga, these carbon–hydrogen complexes must be considered as another potential reservoir for hydrogen. It is important to remember that hydrogen detected in this work only constitutes a fraction of the total hydrogen present. The evolution of hydrogen–acceptor concentrations with illumination and illuminated annealing may not represent the evolution of the total hydrogen introduced into the bulk silicon.

IV. SUMMARY

We have shown that low temperature IR spectroscopy can be used to examine the changes to hydrogen-related point defects in a stack of thin commercially available silicon wafers by increasing the optical path length (~10 mm). In the HPMC-Si wafers examined here, vibrational signatures due to the H–B and H–Ga acceptor complexes, as well as the H_2*(C) complex, were detected in hydrogenated wafers that were subject to a degradation–regeneration cycle representative of the BO-LID and LeTID processes observed in commercial solar cells. Considerably lower concentrations of these hydrogen defects were detected in the nonhydrogenated reference wafer, which is consistent with the observation that LeTID defect complexes require the presence of hydrogen in order to form.

In the HPMC-Si wafers investigated in this study, the concentrations of both H–B and H–Ga decrease *throughout the entire degradation–regeneration process*. While this does not allow us to pinpoint a specific defect as the cause of LeTID, the method demonstrated here can be used to detect and explore the behavior of H-related point defects during various annealing processes.

ACKNOWLEDGMENTS

We are grateful to M. Stavola for useful discussions regarding IR measurements of stacked samples and on hydrogen-related defects in silicon, and to the Department of Physics instrument workshop at the University of Oslo for the design and construction of the sample holder used for the IR measurements. Funding for this work was provided by the Norwegian Research Council through the project *LeTID in multicrystalline PERC cells* (No. 280909) in the EnergiX programme, the Research Center for Sustainable Solar Cell Technology (FME SUSOLTECH, No. 257639), and the Norwegian Micro- and Nano-Fabrication Facility (NorFab, No. 245963).

REFERENCES

[1]S. J. Pearton, J. W. Corbett, and M. Stavola, *Hydrogen in Crystalline Semiconductors* (Springer-Verlag, Heidelberg, 1992).
[2]B. Sopori, Y. Zhang, and N. M. Ravindra, J. Electron. Mater. **30**, 1616 (2001).
[3]A. Azzizi, L. J. Geerligs, and D. H. Macdonald, in *19th EUPVSEC* (WIP, Paris, 2004).
[4]B. J. Hallam, P. G. Hamer, S. Wang, L. Song, N. Nampalli, M. D. Abbott, C. E. Chan, D. Lu, A. M. Wenham, L. Mai, N. Borojevic, A. Li, D. Chen, M. Y. Kim, A. Azmi, and S. Wenham, Energy Procedia **77**, 799 (2015).
[5]M. S. Wiig, H. Haug, R. Søndenå, and E. S. Marstein, Energy Procedia **124**, 215 (2017).
[6]H. Haug, M. S. Wiig, R. Søndenå, B. Ryningen, G. Stokkan, and Ø. Mjøs, in *36th EUPVSEC* (WIP, Marseille, 2019).
[7]B. J. Hallam, P. G. Hamer, A. M. Ciesla née Wenham, C. E. Chan, B. Vicari Stefani, and S. Wenham, "Development of advanced hydrogenation processes for silicon solar cells via an improved understanding of the behaviour of hydrogen in silicon," Prog. Photovolt. Res. Appl. (published online).
[8]R. E. Pritchard, J. H. Tucker, R. C. Newman, and E. C. Lightowlers, Semicond. Sci. Technol. **14**, 77 (1999).
[9]J. C. Muller, Y. Ababou, A. Barhdadi, E. Courcelle, S. Unamuno, D. Salles, P. Siffert, and J. Fally, Sol. Cells **17**, 201 (1986).
[10]M. A. Jensen, A. Zuschlag, S. Wieghold, D. Skorka, A. E. Morishige, G. Hahn, and T. Buonassisi, J. Appl. Phys. **124**, 085701 (2018).
[11]F. Jiang, M. Stavola, A. Rohatgi, D. Kim, J. Holt, H. Atwater, and J. Kalejs, Appl. Phys. Lett. **83**, 931 (2003).
[12]M. Sheoran, D. S. Kim, A. Rohatgi, H. F. W. Dekkers, G. Beaucarne, M. Young, and S. Asher, Appl. Phys. Lett. **92**, 172107 (2008).
[13]A. G. Aberle, Sol. Energy Mater. Sol. Cells **65**, 239 (2001).
[14]S. Wilking, A. Herguth, and G. Hahn, Energy Procedia **38**, 642 (2013).
[15]D. C. Walter and J. Schmidt, Sol. Energy Mater. Sol. Cells **158**, 91 (2016).
[16]A. Ciesla, S. Wenham, R. Chen, C. Chan, D. Chen, B. Hallam, D. Payne, T. Fung, M. Kim, S. Liu, S. Wang, K. Kim, A. Samadi, C. Sen, C. Vargas, U. Varshney, B. V Stefani, P. Hamer, G. Bourret-Sicotte, N. Nampalli, Z. Hameiri, C. Chong, and M. Abbott, in *7th WCPEC* (IEEE, Waikoloa, 2018).
[17]K. Ramspeck, S. Zimmermann, H. Nagel, A. Metz, Y. Gassenbauer, B. Birkmann, and A. Seidel, in *27th EUPVSEC* (WIP, Frankfurt, 2012).
[18]C. Vargas, K. Kim, G. Coletti, D. Payne, C. Chan, S. Wenham, and Z. Hameiri, IEEE J. Photovolt. **8**, 413 (2018).
[19]R. Søndenå and M. S. Wiig, J. Appl. Phys. **125**, 085701 (2019).
[20]R. Eberle, W. Kwapil, F. Schindler, M. C. Schubert, and S. W. Glunz, Phys. Status Solidi Rapid Res. Lett. **10**, 861 (2016).
[21]D. Bredemeier, D. C. Walter, R. Heller, and J. Schmidt, Phys. Status Solidi Rapid Res. Lett. **13**, 1900201 (2019).
[22]D. Bredemeier, D. C. Walter, and J. Schmidt, Sol. Rapid Res. Lett. **2**, 1700159 (2018).
[23]R. Sharma, S. Vajandar, T. Osipowicz, J. B. Li, A. G. Aberle, and Y. Huang, AIP Conf. Proc. **2149**, 140009 (2019).
[24]J. Schmidt, D. Bredemeier, and D. C. Walter, IEEE J. Photovolt. **9**, 1497 (2019).
[25]T. H. Fung, M. Kim, D. Chen, C. E. Chan, B. J. Hallam, R. Chen, D. N. R. Payne, A. Ciesla, S. R. Wenham, and M. D. Abbott, Sol. Energy Mater. Sol. Cells **184**, 48 (2018).
[26]M. A. Jensen, A. E. Morishige, S. Chakraborty, R. Sharma, H. S. Laine, B. Lai, V. Rose, A. Youssef, E. E. Looney, S. Wieghold, J. R. Poindexter, J.-P. Correa-Baena, T. Felisca, H. Savin, J. B. Li, and T. Buonassisi, IEEE J. Photovolt. **8**, 448 (2018).
[27]M. Stavola, S. Kleekajai, L. Wen, C. Peng, V. Yelundur, A. Rohatgi, L. Carnel, and J. Kalejs, Phys. B Condens. Matter **404**, 5066 (2009).
[28]I. L. Kolevatov, P. M. Weiser, E. V. Monakhov, and B. G. Svensson, Phys. Status Solidi Appl. Mater. Sci. **216**, 1800670 (2019).
[29]A. Mainwood and A. M. Stoneham, Phys. B+C **116**, 101 (1983).
[30]A. Mainwood and A. M. Stoneham, J. Phys. C Solid State Phys. **17**, 2513 (1984).
[31]S. J. Pearton, J. W. Corbett, and T. S. Shi, Appl. Phys. A **43**, 153 (1987).
[32]J. W. Corbett, S. N. Sahu, T. S. Shi, and L. C. Snyder, Phys. Lett. A **93**, 303 (1983).
[33]C. Herring, N. M. Johnson, and C. G. Van de Walle, Phys. Rev. B **64**, 125209 (2001).
[34]V. V. Voronkov and R. Falster, Phys. Status Solidi **254**, 1600779 (2017).
[35]P. Hamer, B. Hallam, S. Wenham, and M. Abbott, IEEE J. Photovolt. **4**, 1252 (2014).

[36]M. Stavola, *Identification of Defects in Semiconductors*(Academic Press, Boston, MA, 1998), Vol. 51B.
[37]M. Stavola and W. B. Fowler, J. Appl. Phys. **123**, 161561 (2018).
[38]A. Nakanishi, N. Fukata, and M. Suezawa, Phys. B Condens. Matter **308–310**, 216 (2001).
[39]J. Mullins, V. P. Markevich, M. P. Halsall, and A. R. Peaker, Phys. Status Solidi **216**, 1800611 (2019).
[40]M. Stavola, S. J. Pearton, J. Lopata, and W. C. Dautremont-Smith, Appl. Phys. Lett. **50**, 1086 (1987).
[41]K. Bergman, M. Stavola, S. J. Pearton, and J. Lopata, Phys. Rev. B **37**, 2770 (1988).
[42]J.-F. Zheng and M. Stavola, Phys. Rev. Lett. **76**, 1154 (1996).
[43]C. Peng, H. Zhang, M. Stavola, V. Yelundur, A. Rohatgi, L. Carnel, M. Seacrist, and J. Kalejs, J. Appl. Phys. **109**, 053517 (2011).
[44]B. Hourahine, R. Jones, S. Öberg, P. R. Briddon, V. P. Markevich, R. C. Newman, J. Hermansson, M. Kleverman, J. L. Lindström, L. I. Murin, N. Fukata, and M. Suezawa, Phys. B Condens. Matter **308–310**, 197 (2001).
[45]D. C. Walter, D. Bredemeier, R. Falster, V. V. Voronkov, and J. Schmidt, Sol. Energy Mater. Sol. Cells **200**, 109970 (2019).
[46]A.-K. Søiland, J. O. Odden, B. Sandberg, K. Friestad, J. Håkedal, E. Enebakk, and S. Braathen, in *CSSC-6* (Aix-Les-Bains, 2012).
[47]H. Haug, R. Søndenå, M. S. Wiig, and E. S. Marstein, Energy Procedia **124**, 47 (2017).
[48]T. Trupke, R. A. Bardos, M. C. Schubert, and W. Warta, Appl. Phys. Lett. **89**, 044107 (2006).
[49]F. Wolny, A. Krause, A. Oehlke, and M. Wagner, Energy Procedia **92**, 274 (2016).
[50]S. A. McQuaid, R. C. Newman, J. H. Tucker, E. C. Lightowlers, R. A. A. Kubiak, and M. Goulding, Appl. Phys. Lett. **58**, 2933 (1991).
[51]R. Søndenå, H. Haug, C. C. You, J. Zhu, and M. S. Wiig, AIP Conf. Proc. **2149**, 140010 (2019).
[52]J. L. McAfee and S. K. Estreicher, Phys. B Condens. Matter **340–342**, 637 (2003).
[53]R. Søndenå, H. Haug, A. Song, C.-C. Hsueh, and J. O. Odden, AIP Conf. Proc. **1999**, 130016 (2018).
[54]E. V. Lavrov, L. Hoffmann, B. Bech Nielsen, B. Hourahine, R. Jones, S. Öberg, and P. R. Briddon, Phys. Rev. B **62**, 12859 (2000).
[55]R. E. Pritchard, M. J. Ashwin, J. H. Tucker, and R. C. Newman, Phys. Rev. B **57**, R15048 (1998).
[56]A. W. R. Leitch, V. Alex, and J. Weber, Phys. Rev. Lett. **81**, 421 (1998).
[57]E. E. Chen, M. Stavola, W. B. Fowler, and P. Walters, Phys. Rev. Lett. **88**, 105507 (2002).
[58]M. Stavola, E. E. Chen, W. B. Fowler, and G. A. Shi, Phys. B Condens. Matter **340–342**, 58 (2003).
[59]R. E. Pritchard, M. J. Ashwin, J. H. Tucker, R. C. Newman, E. C. Lightowlers, M. J. Binns, S. A. McQuaid, and R. Falster, Phys. Rev. B **56**, 13118 (1997).
[60]E. E. Chen, M. Stavola, and W. B. Fowler, Phys. Rev. B **65**, 245208 (2002).
[61]P. Stallinga, P. Johannesen, S. Herstrøm, K. Bonde Nielsen, B. Bech Nielsen, and J. R. Byberg, Phys. Rev. B **58**, 3842 (1998).
[62]M. Suezawa, Phys. Rev. B **63**, 35201 (2000).
[63]M. Budde, *Hydrogen-Related Defects in Proton-Implanted Silicon and Germanium: An Infrared Absorption Spectroscopy Study* (University of Aarhus, 1998).
[64]B. Bech Nielsen, L. Hoffmann, M. Budde, R. Jones, J. P. Goss, and S. Öberg, Mater. Sci. Forum **196–201**, 933 (1995).
[65]M. U. Khan, D. Chen, S. Jafari, T. Ohshima, H. Abe, Z. Hameiri, C. M. Chong, and M. Abbott, Sol. Energy Mater. Sol. Cells **200**, 109990 (2019).
[66]C. P. Herrero, M. Stutzmann, and A. Breitschwerdt, Phys. Rev. B **43**, 1555 (1991).
[67]M. Stavola, S. J. Pearton, J. Lopata, and W. C. Dautremont-Smith, Phys. Rev. B **37**, 8313 (1988).